



2017

Bolstering cholesteryl ester hydrolysis in liver: A hepatocyte-targeting gene delivery strategy for potential alleviation of atherosclerosis

Hongliang He

Virginia Commonwealth University

Michael G. Lancina III

Virginia Commonwealth University

Jing Wang

Virginia Commonwealth University

See next page for additional authors

Follow this and additional works at: http://scholarscompass.vcu.edu/chem_pubs

 Part of the [Chemistry Commons](#)

(C) 2017 Elsevier Ltd. All rights reserved.

Downloaded from

http://scholarscompass.vcu.edu/chem_pubs/72

This Article is brought to you for free and open access by the Dept. of Chemistry at VCU Scholars Compass. It has been accepted for inclusion in Chemistry Publications by an authorized administrator of VCU Scholars Compass. For more information, please contact libcompass@vcu.edu.

Authors

Hongliang He, Michael G. Lancina III, Jing Wang, William J. Korzun, Hu Yang, and Shobha Ghosh



Bolstering cholesteryl ester hydrolysis in liver: A hepatocyte-targeting gene delivery strategy for potential alleviation of atherosclerosis



Hongliang He^a, Michael G. Lancina III^b, Jing Wang^c, William J. Korzun^d, Hu Yang^{a, e, f, *}, Shobha Ghosh^{c, **}

^a Department of Chemical and Life Science Engineering, Virginia Commonwealth University, Richmond, VA, 23219, United States

^b Department of Biomedical Engineering, Virginia Commonwealth University, Richmond, VA, 23284, United States

^c Department of Internal Medicine, Virginia Commonwealth University, Richmond, VA, 23298, United States

^d Department of Clinical Laboratory Sciences, Virginia Commonwealth University, Richmond, VA, 23298, United States

^e Department of Pharmaceutics, Virginia Commonwealth University, Richmond, VA, 23298, United States

^f Massey Cancer Center, Virginia Commonwealth University, Richmond, VA, 23298, United States

ARTICLE INFO

Article history:

Received 20 January 2017

Received in revised form

17 March 2017

Accepted 17 March 2017

Available online 26 March 2017

Keywords:

Atherosclerosis

PAMAM dendrimer

Galactose

CEH

Hepatocyte targeting

Gene delivery

ABSTRACT

Current atherosclerosis treatment strategies primarily focus on limiting further cholesteryl esters (CE) accumulation by reducing endogenous synthesis of cholesterol in the liver. No therapy is currently available to enhance the removal of CE, a crucial step to reduce the burden of the existing disease. Given the central role of hepatic cholesteryl ester hydrolase (CEH) in the intrahepatic hydrolysis of CE and subsequent removal of the resulting free cholesterol (FC), in this work, we applied galactose-functionalized polyamidoamine (PAMAM) dendrimer generation 5 (Gal-G5) for hepatocyte-specific delivery of CEH expression vector. The data presented herein show the increased specific uptake of Gal-G5/CEH expression vector complexes (simply Gal-G5/CEH) by hepatocytes *in vitro* and *in vivo*. Furthermore, the upregulated CEH expression in the hepatocytes significantly enhanced the intracellular hydrolysis of high density lipoprotein-associated CE (HDL-CE) and subsequent conversion/secretion of hydrolyzed FC as bile acids (BA). The increased CEH expression in the liver significantly increased the flux of HDL-CE to biliary as well as fecal FC and BA. Meanwhile, Gal-G5 did not induce hepatic or renal toxicity. It was also not immunotoxic. Because of these encouraging pre-clinical testing results, using this safe and highly efficient hepatocyte-specific gene delivery platform to enhance the hepatic processes involved in cholesterol elimination is a promising strategy for the alleviation of atherosclerosis.

© 2017 Elsevier Ltd. All rights reserved.

1. Introduction

Cardiovascular disease (CVD) continues to be the number one cause of morbidity and mortality in the Western World including the USA [1,2]. The most common cause of CVD is atherosclerosis characterized with deposition of cholesteryl ester (CE)-laden macrophage foam cells in the arterial wall, a process starting in the teenage years and progressing silently for years before the manifestation of clinical symptoms [3,4]. A common therapeutic strategy is to reduce plasma cholesterol by restricting cholesterol intake or

reducing *de novo* cholesterol biosynthesis. The rationale behind this strategy is to reduce the influx of cholesterol into the macrophages, hence reducing new foam cell formation and halting the plaque progression. Nonetheless, to reduce the lipid burden in the existing plaque, the only plausible way is to enhance the removal of CE from the macrophage foam cells [5]. Furthermore, reduction in the lipid core of the plaques may help increase plaque stability, hence likely reducing acute cardiovascular events such as heart attacks [6]. Although the importance of increasing the flux of cholesterol from macrophages to the liver for final elimination (or reverse cholesterol transport, RCT) is widely recognized, no therapy is available to enhance the removal of CE from the existing plaques, facilitate plaque regression, or increase plaque stability [7].

Under a normal physiological setting, a homeostatic balance between cholesterol influx (unregulated uptake of modified low density lipoprotein (mLDL)) and efflux (removal of un-esterified or

* Corresponding author. Department of Chemical and Life Science Engineering, Virginia Commonwealth University, Richmond, VA, 23219, United States.

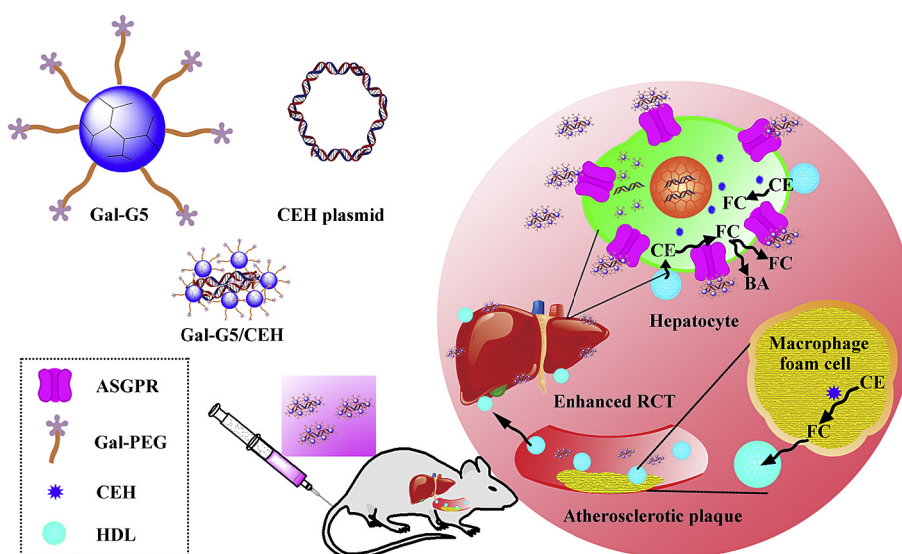
** Corresponding author. Department of Internal Medicine, Virginia Commonwealth University, Richmond, VA, 23298, United States.

E-mail addresses: hyang2@vcu.edu (H. Yang), shobha@vcu.edu (S. Ghosh).

free cholesterol (FC) by apolipoprotein A1, ApoA1 or high density lipoprotein (HDL) restricts pathological accumulation of CE in macrophages. However, a disrupted balance between cholesterol influx and efflux leads to excessive accumulation of CE within the macrophage foam cells, causing pathological consequences. With the failure to show any therapeutic improvement in clinical trials aimed at increasing HDL cholesterol by niacin (AIM-HIGH and HPS2-THRIVE (Heart Protection Study 2-Treatment of HDL to Reduce the Incidence of Vascular Events)) or cholesterol ester transfer protein (CETP) inhibitor [8], focus has recently shifted to the efflux ability of HDL to remove cholesterol from macrophage foam cells [4]. Correlation between the HDL efflux capacity and CVD has been established clinically [9–11]. It must be noted that although macrophage foam cells store cholesterol in the form of CE, only FC is available for efflux to ApoA1 or HDL via the membrane cholesterol transporters ABCA1 (ATP Binding Cassette Subfamily A Member 1) and ABCG1 (ATP Binding Cassette Subfamily G Member 1), thus making intracellular CE hydrolase (CEH)-mediated conversion of CE into FC an important and likely rate-limiting step in cholesterol efflux pathway [12,13].

Liver is the central organ for the clearance of cholesterol from the body. Cholesterol removed from the peripheral organs including plaque associated macrophages returns to the liver via HDL, which contains >80% of cholesterol in the form of CE [14]. HDL receptor scavenger receptor class B type I (SR-BI) on the hepatocyte surface facilitates the selective delivery of HDL-associated CE (HDL-CE) and FC. While HDL-FC is thought to be rapidly secreted into bile, the fate of HDL-CE is not completely defined [7]. We have confirmed that hepatic CEH plays a central role in HDL-CE hydrolysis. We observed that liver-specific transgenic expression of human liver CEH enhanced the flux of HDL-CE to bile and feces and reduced Western-diet induced atherosclerosis [15–17]. Enhanced bile acid secretion was found to reduce the CVD risk [18,19]. These studies validated the unidirectional flux of cholesterol from macrophage foam cells to the liver and to bile/feces as an anti-atherogenic step. Therefore, novel anti-atherogenic agents can be developed to promote hepatic hydrolysis of HDL-CE. Liver-specific delivery of CEH gene represents one such approach.

With these concepts in mind, here we used polyamidoamine (PAMAM) dendrimer generation 5 (G5) to design a hepatocyte-specific delivery system to deliver CEH expression vector and enhance its expression in the liver so as to increase the final elimination of cholesterol (See Scheme 1). PAMAM dendrimers have distinct merits as non-viral gene delivery vectors, including well-defined nanoscale spherical architecture, large number of surface amine groups capable of efficiently complexing with genes through electrostatic interactions, as well as endosomal-lysosomal escape ability due to the proton-sponge effect [20–23]. Moreover, PAMAM dendrimers have been widely modified with various targeted ligands, such as carbohydrate moieties [24], antibodies [25], peptides [26] and aptamers [27] to enhance targeting specificity. Although the majority of cells (60–80%) in the liver are parenchymal hepatocytes, most nanoparticles are typically taken up by non-parenchymal Kupffer cells (mononuclear phagocyte system, MPS) [28–30]. Thus, maximizing the active uptake by hepatocytes meanwhile minimizing the passive clearance by the MPS in the liver is an important consideration for development of hepatocyte-specific non-viral gene delivery platforms [31,32]. Taking advantage of hepatocyte-specific expression of asialoglycoprotein receptor (ASGPR) and the strong affinity of this receptor for galactose [33–35], G5 was functionalized with galactose (Gal) via a long polyethylene glycol (PEG) spacer (35 kDa) to form Gal-G5, where long PEG spacer will likely reduce the toxicity from the enormous G5 surface cations. Liver-targeted anticancer drug delivery using lactobionic acid-functionalized dendrimers has been reported [36,37]. For the first time, we used Gal-functionalized PAMAM dendrimer for liver-specific gene delivery. The data presented here demonstrate specific uptake of Gal-G5 by hepatocytes *in vitro* and *in vivo*. Furthermore, we confirmed the ability of Gal-G5 to efficiently deliver CEH expression vector and increase the hepatic hydrolysis of HDL-CE to FC and subsequently to bile acids. Development of such a safe, liver hepatocyte-specific efficient dendrimer-based delivery system for CEH expression vector offers a possible solution to regressing the existing atherosclerotic plaques.



Scheme 1. Design of a hepatocyte-specific anti-atherogenic gene delivery system. Cholesterol (>80% in the form of CE) is transported by HDL from atherosclerotic plaque-associated macrophage foam cells to the liver by the process of RCT, subsequently converted to BA, and eliminated from bile/feces. Galactose-functionalized PAMAM dendrimer G5, i.e., Gal-G5, is developed as a hepatocyte-specific gene delivery system to deliver CEH expression vector. Galactose facilitates ASGPR-mediated endocytosis of Gal-G5/CEH complexes into hepatocytes in the liver and increases CEH expression. The overexpressed CEH would enhance the hydrolysis of HDL-CE into FC, which is either directly secreted into bile or converted to bile acids followed by elimination from the body - a process proposed to regress the existing atherosclerotic plaques.

2. Materials and methods

2.1. Materials

Ethylenediamine (EDA) core PAMAM dendrimer G5 (technical grade) was purchased from Dendritech (Midland, MI). Fluorescein isothiocyanate (FITC) and D-(+)-galactose were purchased from Sigma-Aldrich (St. Louis, MO). IRDye 800CW NHS ester was obtained from Li-COR Biotechnology (Lincoln, NE). Galactose-PEG-NHS ($M_n = 35000$ g/mol) was purchased from JenKem Technology (Plano, TX, USA). SnakeSkin dialysis tubing with 7000 molecular weight cut-off (MWCO) was purchased from Thermo Scientific (Rockford, IL). Water soluble tetrazolium-1 (WST-1) reagent was purchased from Roche Applied Science (Grand Island, NY). Collagenase type I was obtained from Worthington Biochemical Corp. William's E medium. Fetal bovine serum (FBS) and Dulbecco's phosphate-buffered saline (DPBS) were obtained from Gibco BRL (Carlsbad, CA, USA). Trypsin-EDTA (0.25%), streptomycin and penicillin were obtained from Invitrogen Co., USA. Label IT[®] Cy3 control plasmid was purchased from Mirus Bio (Madison, WI). Vectashield mounting media were purchased from Vector Laboratories (Burlingame, CA). RNeasy[®] Mini Kit was purchased from QIAGEN GmbH. High Capacity cDNA Reverse Transcription Kit and TaqMan Universal PCR Master Mix, no AmpErase UNG were obtained from Applied Biosystems. Human macrophage CEH plasmid (Accession No. AY268104, referred to as CEH hereafter) was constructed and characterized in our lab [38]. Unless noted, the rest chemicals were purchased from Sigma-Aldrich (St. Louis, MO).

2.2. Animals

Six-week-old C57BL/6 mice (20 ± 3 g body weight, both genders) were obtained from the Jackson Laboratory (Bar Harbor, ME). All the mice were kept in pathogen-free conditions with 12 h dark/light cycle. All procedures were approved by the Virginia Commonwealth University Institutional Animal Care and Use Committee.

2.3. Isolation and culture of primary mouse hepatocytes

Primary mouse hepatocytes were isolated by collagenase-perfusion technique as described previously [39]. The hepatocytes were plated in collagen-coated wells in William's E medium supplemented with heat-inactivated FBS (10%), insulin (1.5 μ M), streptomycin (100 U/mL) and penicillin (100 U/mL). After 3 h, the medium containing detached dead cells was aspirated and replaced with fresh medium prior to any treatment. Unless noted, hepatocytes at ~90% confluence were used throughout the experiments.

2.4. Evaluation of Gal-G5

2.4.1. Synthesis and characterization

Fifteen mg of PAMAM dendrimer G5 was dissolved in 0.1 M sodium bicarbonate solution (pH 8.3–8.5) (10 mL), to which was added 275 mg of Galactose-PEG-NHS (the molar ratio of Galactose-PEG-NHS to G5 was approximately 15:1). The reaction proceeded overnight at room temperature followed by dialysis and lyophilization to obtain Gal-G5. Following the same chemistry, Gal-G5 and G5 were reacted with IRDye 800CW NHS ester to form IRDye 800CW-labeled Gal-G5 and IRDye 800CW-labeled G5. To monitor intracellular uptake and trafficking *in vitro*, Gal-G5 and G5 were labeled with FITC following a reported procedure [40]. ¹H NMR spectra were recorded on a Varian superconducting Fourier-transform NMR spectrometer (Mercury-300) [20]. D₂O was used as the solvent.

2.4.2. Cytotoxicity assessment

Primary mouse hepatocytes were seeded in 48-well collagen-coated cell culture plates ($n = 6$) at a density of 5×10^4 cells/well and cultured in William's E medium containing 10% FBS overnight. The cells were then incubated with increasing concentrations of Gal-G5 or G5 (1–500 nM) for an additional 24 h, washed with DPBS three times, and then subjected to WST-1 assay. In a separate experiment, hepatocytes were treated 100 nM Gal-G5 or G5 for 24 h, rinsed with DPBS, stained with cell-impermeable fluorescent dye (DAPI) for 30 s, washed with DPBS again three times, and imaged.

2.4.3. *In vitro* uptake by hepatocytes

Primary mouse hepatocytes were incubated with 50 nM FITC-Gal-G5 or FITC-G5 for various lengths of time (2, 8, or 24 h). At the end of each treatment, the cells were washed with DPBS three times, fixed with 4% buffered formalin PBS at room temperature for 30 min, and permeabilized with 0.15% Triton X-100 for 5 min. The cells were washed with DPBS three times, counterstained with DAPI, and imaged using a fluorescence microscope.

In a separate experiment, primary mouse hepatocytes cultured in the collagen-coated 60-mm dishes were incubated with 50 nM FITC-Gal-G5 or FITC-G5 for 2, 8 or 24 h. At the end of each treatment, the hepatocytes were collected and analyzed by using Canto-BD FACSCanto™ II Analyzer (BD, USA) for quantification of nanoparticle uptake in terms of mean fluorescence intensity (MFI).

2.4.4. Competitive inhibition assay

Primary mouse hepatocytes were seeded on 4-chamber slides, cultured overnight, and incubated with free galactose (0, 3 or 30 μ M) for 30 min followed by addition of 50 nM FITC-Gal-G5. After 2 h, the cells were counterstained with DAPI and imaged by using fluorescent microscopy. An identical experiment was conducted, and the cells were collected for quantitative analysis of nanoparticle uptake by using flow cytometry.

2.4.5. Uptake by mouse peritoneal macrophages

Mouse peritoneal macrophages were isolated following a published protocol [41]. The cell pellets were collected after centrifugation at 2000 rpm for 5 min, re-suspended in William's E medium supplemented with 10% FBS and 1% antibiotics and plated. The non-adherent cells were removed after 2 h. The cells were incubated with 50 nM FITC-G5 or FITC-Gal-G5 for 6 h and then processed for fluorescence imaging and flow cytometry.

2.5. *In vitro* evaluation of Gal-G5/CEH complexes

2.5.1. Gel retardation assay

Gal-G5/CEH complexes (2.5, 5, 10, 20, 40 and 50, w/w) and G5/CEH (0.25, 0.5, 1, 2, 4 and 8, w/w) were prepared following a procedure described earlier [23,42]. The complexes were mixed with loading buffer and loaded onto a 0.8% agarose gel containing ethidium bromide. The 1 kb DNA ladder (New England Biolabs, Ipswich, MA) was included as a control. Electrophoresis was performed in Tris-acetate-EDTA buffer at 100 V for 40 min. The DNA bands were visualized with a UV-light system.

2.5.2. Colloidal stability test

Gal-G5/CEH (20:1, w/w) and G5/CEH (4:1, w/w) were used in the rest studies. The hydrodynamic diameters of freshly prepared complexes were measured at room temperature using a Malvern Zetasizer Nano ZS90 (Malvern Instruments, Worcestershire, UK). Furthermore, their size change during 24 h-incubation at 37 °C was monitored. The colloidal stability of the complexes following 24 h-incubation at 37 °C in PBS or PBS with 10% FBS was examined using

gel retardation assay.

2.5.3. Transmission electron microscopy (TEM)

Gal-G5 and Gal-G5/CEH (20:1, w/w) sample suspensions were loaded onto a 300 mesh carbon coated copper grid, air dried at room temperature, and imaged under a transmission electron microscope (TEM) (JEM-3010, JEOL, Tokyo, Japan).

2.5.4. Intracellular trafficking study

Label IT[®] Cy3[®] plasmid delivery control (referred to as Cy3 plasmid hereafter) was used a control. Hepatocytes were seeded in 2-well chamber slides and allowed to attach overnight. The cells were incubated with FITC-Gal-G5/Cy3 plasmid (5 µg/0.25 µg) or FITC-G5/Cy3 plasmid (1 µg/0.25 µg) in 500 µL of William's E medium with 10% FBS at 37 °C for 6 h. Afterwards, the medium in each chamber was replaced with fresh growth medium containing 10% FBS. The cells were cultured for an additional 6 or 24 h. At the end of incubation, the cells were rinsed with DPBS, fixed with 4% buffered formalin PBS, permeabilized with 0.15% Triton X-100 and counterstained with DAPI. The cells were then imaged under a Zeiss LSM 700 confocal laser scanning microscope.

2.5.5. Transfection and biological activity studies

Hepatocytes were cultured in 6-well plates (~90% confluence) and transfected with Gal-G5/CEH (5 µg/0.25 µg), Gal-G5/empty control vector (pCMV) (5 µg/0.25 µg), G5/CEH (1 µg/0.25 µg), or G5/pCMV (1 µg/0.25 µg) in William's E medium with 10% FBS for 24 h. After the medium in each well was replaced with fresh growth medium containing 10% FBS, the cells were cultured for an additional 24 or 48 h. CEH mRNA expression was quantified using reverse transcription quantitative PCR (RT-qPCR) as described our previous work [15,43,44]. CEH mRNA expression-mediated by Gal-G5 or G5 relative to the expression observed in the hepatocytes transfected with pCMV-mediated with the same carrier was determined. CEH enzymatic activity was determined by monitoring the intracellular hydrolysis of HDL-delivered ³H-CE (HDL-³H-CE) that was added to a separate set of hepatocytes following 24 h-transfection. CEH enzymatic activity was assessed in terms of ³H-FC accumulation in the cells, and the effects of increased CEH expression on flux of HDL-³H-CE to bile acids was assessed by monitoring the release of ³H-bile acids (³H-BA) in the medium as described earlier [15,43]. CEH enzymatic activity in non-transfected hepatocytes was examined as control.

2.6. In vivo studies

2.6.1. Biodistribution

IRDye 800CW-labeled Gal-G5/CEH (20:1, w/w) or IRDye 800CW-labeled G5/CEH (4:1, w/w) was administered to C57BL/6 mice via tail vein injection. Both formulations were adjusted to have an equivalent amount of total fluorescent intensity (0.5 mg IRDye 800CW/kg in 0.2 mL, balanced in osmolality with the addition of DPBS). At each pre-determined time point up to 168 h, a group of 3 mice for each formulation were euthanized. Major organs (heart, liver, spleen, lung and kidney) were harvested and imaged using an Odyssey[®] Fc Imaging System (LI-COR, Nebraska USA) at ex/em = 780/800 nm followed by quantitative image analysis of fluorescence signals [45–47].

2.6.2. Tissue analysis of CEH mRNA expression

C57BL/6 mice received a bolus dose of Gal-G5/CEH (20:1, w/w) or G5/CEH (4:1, w/w) (n = 3) via tail vein injection (0.3 mg CEH/kg in 200 µL, balanced in osmolality with the addition of DPBS) via tail vein. At 24, 48, and 72 h-post injection, a group of 3 mice for each formulation were sacrificed. The major organs (heart, liver, lung,

kidney, and spleen) were harvested and processed for quantification of CEH gene expression using RT-qPCR. To distinguish CEH expression between hepatocytes and resident macrophages (i.e., Kupffer cells) in the liver, one extra group of 3 mice treated with Gal-G5/CEH or G5/CEH were sacrificed at 48 h-post injection, and the hepatocytes and Kupffer cells in the liver were isolated and subjected to RT-qPCR analysis [48].

2.6.3. Acute toxicity studies

C57BL/6 mice received a bolus dose of Gal-G5/CEH (20:1, w/w) or G5/CEH (4:1, w/w) (0.6 mg CEH/kg) (n = 3 per group) via tail vein injection and maintained on chow diet. Untreated C57BL/6 mice (n = 3) were included as control. The mice were sacrificed at 24 h-post administration. To assess hepatic toxicity, renal toxicity and immunotoxicity of the formulations, the blood was collected and analyzed for aspartate aminotransferase (AST), alanine aminotransferase (ALT), blood urea nitrogen (BUN), interleukin 6 (IL-6) and tumor necrosis factor-α (TNF-α) [33]. The tissues (heart, liver, spleen, lung, and kidney) were processed for hematoxylin and eosin (H&E) staining.

2.6.4. Flux of HDL-³H-CE to feces

C57BL/6 mice received a bolus dose of Gal-G5/CEH (20:1, w/w) (0.6 mg CEH/kg) or plain Gal-G5 (12 mg/kg, equivalent to that used in the Gal-G5/CEH group) (n = 3 per group) via tail vein injection and maintained on chow diet. At 48 h-post injection, one dose of HDL-³H-CE (1.63 × 10⁶ dpm/mouse) was administered to the mice via tail vein injection. The mice were transferred to metabolic cages and maintained for an additional 48 h until they were euthanized. The blood, whole liver, gall bladder bile as well as feces were collected. CEH expression in the liver was quantified with RT-qPCR. Total radio activity in plasma, liver, and gall bladder was quantified [48]. Furthermore, ³H-BA and ³H-FC were extracted from liver, gall bladder bile and feces and quantified [15,17,49].

2.7. Statistical analysis

The data are expressed as mean ± SD. Student's t-test was used for statistical analysis, and P < 0.05 was considered statistically significant.

3. Results and discussions

3.1. Synthesis and characterization of Gal-G5

Gal-G5 (Fig. 1A) was synthesized by directly coupling Gal-PEG-NHS to PAMAM G5 via NHS ester-amine reaction. ¹H NMR was used to check the purity and conjugation of galactose-modified dendrimer. The spectrum (Fig. 1B) confirms the relative high purity of the synthesized Gal-G5 as interfering proton peaks from reactants, intermediates, or reaction solvent are not seen. The methylene protons of branching units of G5 has multiple peaks between 2.2 and 3.4 ppm. The repeat units of PEG from Gal-PEG-NHS has a singlet peak at 3.6 ppm. According to the proton peak integration, an average of 11 Gal-PEG chains were conjugated to G5.

Gal-G5 showed enhanced cytocompatibility. It remained nontoxic to hepatocytes when the concentration was increased to 100 nM (Fig. 2A). In contrast, the toxicity of G5 at 100 nM was strong, causing cell viability to drop to 62%. The cell viability was further decreased to 30% by G5 at 500 nM. In contrast, 65% of the cells remained viable in the presence of 500 nM Gal-G5, indicating its relatively higher cytocompatibility. After DAPI staining, a significant fraction of dead cells are clearly seen in the G5/100 nM group (Fig. 2B), whereas such observation is not seen in the Gal-G5/100 nM group. Galactose functionalized G5 obtained significantly

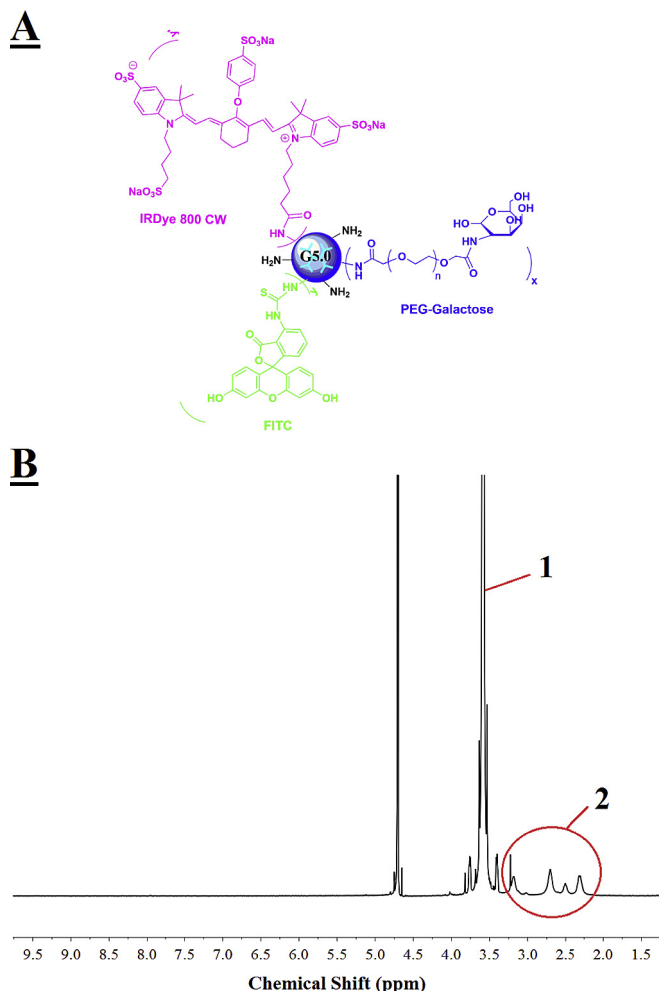


Fig. 1. Chemical structure and characterization of Gal-G5. (A) PAMAM dendrimer G5 functionalized with hepatocyte specific ligand galactose alone or along with fluorescence dye (FITC or IRDye 800CW). (B) 300 MHz ¹H NMR spectrum of Gal-G5 in D₂O. Multiple proton peaks 2 between 2.2 and 3.4 ppm are assigned to the methylene protons of G5 branching units, while a singlet peak 1 at 3.6 ppm is assigned to the ethylene protons of the repeat units of PEG. D₂O has a proton peak at 4.8 ppm.

improved cytocompatibility likely due to the effective charge shielding effect of PEG chains and decreased number of amines on the dendrimer surface as reported in the literature [50–52].

3.2. Hepatocyte-specificity of Gal-G5 *in vitro*

Cellular uptake kinetics of FITC-G5 (50 nM) and FITC-Gal-G5

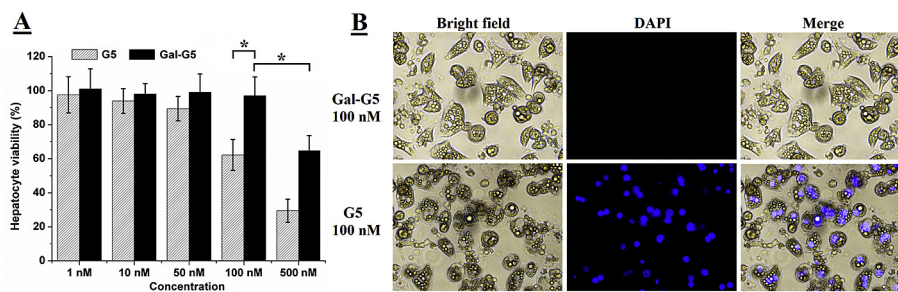


Fig. 2. Gal-G5 shows high cytocompatibility. Primary mouse hepatocytes were treated with Gal-G5 or G5 at the indicated concentrations for 24 h and then assessed with the WST-1 assay for viability. (A) Gal-G5 is more tolerated by primary mouse hepatocytes. *P < 0.05 (n = 5). (B) Representative images of the cells treated with G5 or Gal-G5 at 100 nM. The cells stained with fluorescent dye DAPI are dead cells due to the lack of an intact cell membrane. Scale bar: 20 μm.

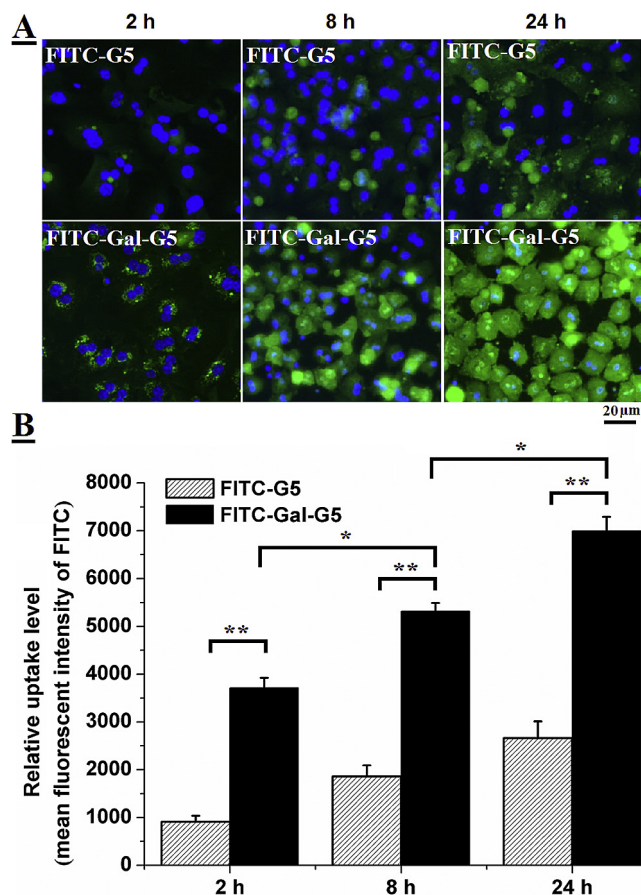


Fig. 3. Gal-G5 shows enhanced uptake by hepatocytes. Primary mouse hepatocytes were incubated with 50 nM FITC-Gal-G5 or FITC-G5 for various lengths of time (2, 8, or 24 h) and then subjected to fluorescence imaging and flow cytometry analysis. (A) Representative fluorescence images. (B) Quantification of nanoparticle uptake as a function of time reported as MFI of FITC. n = 3, *P < 0.05, **P < 0.01.

(50 nM) by primary hepatocytes was monitored by using fluorescence microscopy (Fig. 3A). Increased cellular uptake of nanoparticles with increasing incubation time was observed in both groups, but a much stronger fluorescence signal was seen in the FITC-Gal-G5 group at any time point as compared to FITC-G5. Consistent with the imaging data, FITC-Gal-G5 shows much higher cellular uptake (measured as mean fluorescent intensity, MFI) (Fig. 3B). For instance, the MFI of FITC-Gal-G5 is 7000 ± 300 at 24 h, which is ten-fold stronger than that of FITC-G5.

The uptake of FITC-Gal-G5 via ASGPR was confirmed using competitive inhibition assay. As shown in Fig. 4A, fluorescence

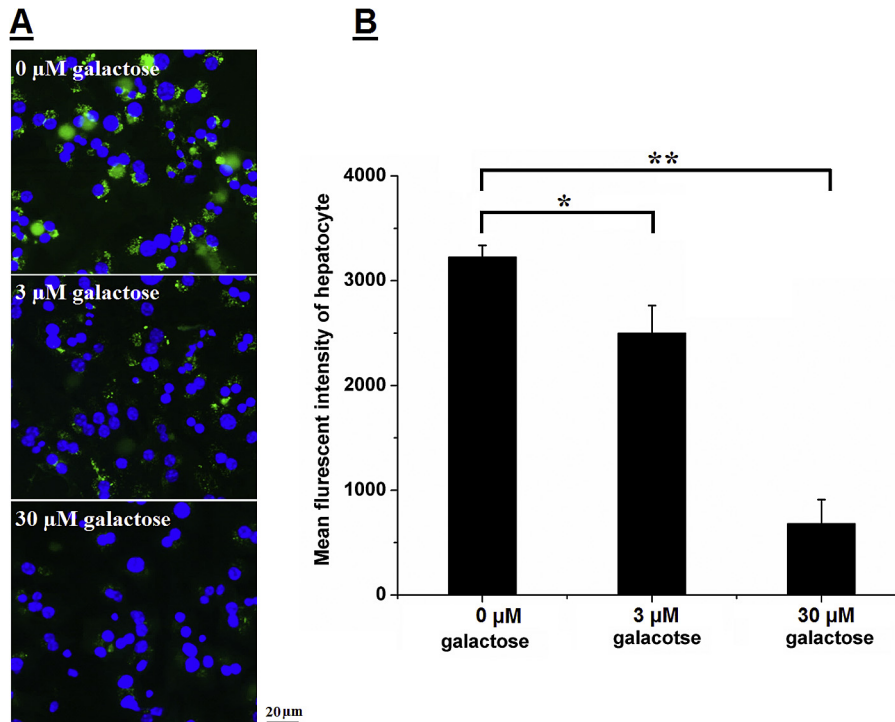


Fig. 4. Receptor-mediated endocytosis of Gal-G5 by hepatocytes: competitive inhibition study. Freshly isolated mouse hepatocytes were pre-incubated with galactose (0, 3, or 30 μM) for 30 min at 37 °C and then with 50 nM Gal-G5 for 2 h. The uptake of FITC-Gal-G5 was monitored by fluorescence microscopy (A) and quantified by flow cytometry (B). n = 3, *P < 0.05, and **P < 0.01.

signal of FITC-Gal-G5 was reduced significantly with increasing exogenous galactose concentration. Flow cytometry was used to quantify the uptake, and the MFI values are shown in Fig. 4B. Compared to the uptake observed in the absence of galactose, significantly reduced uptake was seen in the presence of 3 μM free galactose (24% decrease, P < 0.05) and 30 μM (77% decrease, P < 0.01). Free galactose selectively binds ASGPR. The presence of free galactose suppressed the uptake of FITC-Gal-G5 because it bound to the receptors and blocked the access of FITC-Gal-G5 to the same receptors. These data clearly demonstrate that the galactose functionalization of G5 effectively increased the uptake by hepatocytes through the ASGPR that has a high affinity for galactose. These observations are consistent with other studies reporting galactose-mediated increase in hepatocyte uptake of nanoparticles [53–55].

Additionally, the effect of galactose modification on the uptake of G5 by mouse peritoneal macrophages, one of the most aggressive scavengers, was investigated. The results showed that the uptake of Gal-G5 by macrophages was 4-fold lower than that of plain G5 (Fig. 5A and 5B). The reduced uptake by macrophages is likely due to low expression of galactose receptor ASGPR on the macrophages. In addition, PEGylation of Gal-G5 helped reduce non-specific uptake due to the surface charge shielding effect [56–59].

3.3. Characterization of dendrimer/CEH complexes

Formation of dendrimer/CEH complexes was initially evaluated by using gel retardation assay. As shown in Fig. 6A, G5 and CEH plasmid form stable complexes at a weight ratio of 4 or higher. A weight ratio of 20 or higher is needed for Gal-G5 to complex with CEH plasmid stably, presumably due to the charge shielding effect of long PEG chains evidenced by zeta potential decrease from 30 mV for G5 to 2 mV for Gal-G5. Nonetheless, the DNA compaction

ability of Gal-G5 is deemed sufficient. Hydrodynamic size results (Fig. 6B) show that size significantly increased from ~10 nm for Gal-

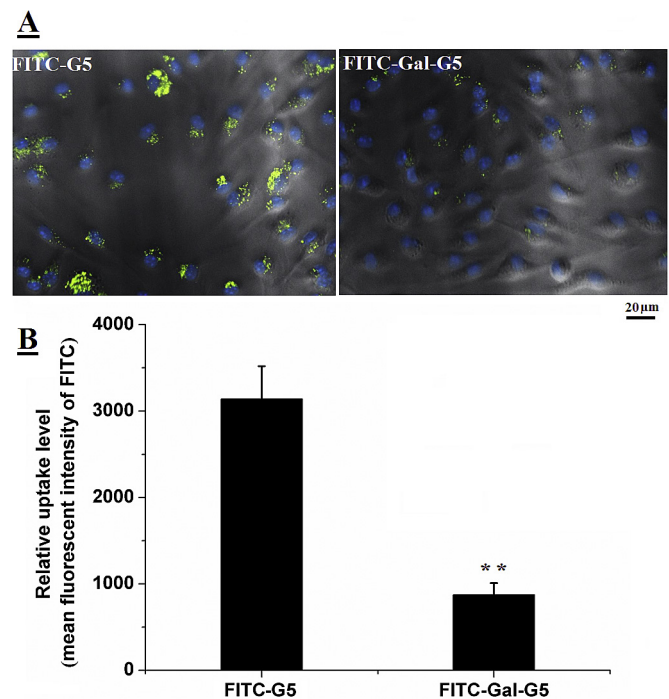


Fig. 5. Gal-G5 shows reduced uptake by macrophages. Mouse peritoneal macrophages were incubated with 50 nM FITC-Gal-G5 or FITC-G5 for 6 h and then subjected to fluorescence imaging or flow cytometry analysis. (A) Representative fluorescence images. (B) Quantification of nanoparticle uptake reported as MFI of FITC. n = 3, **P < 0.01.

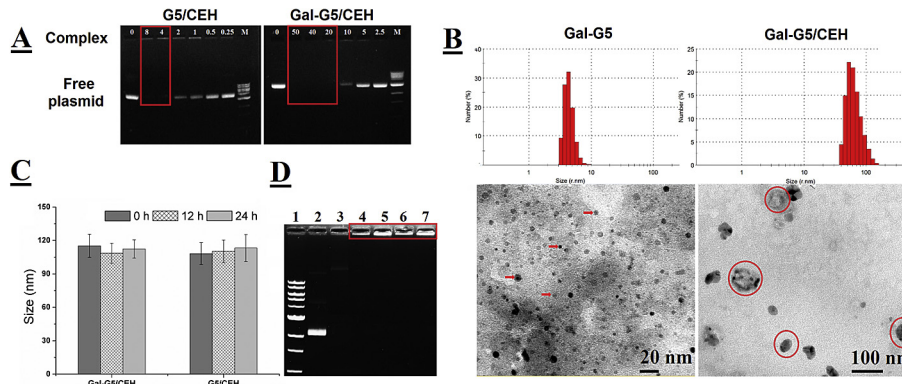


Fig. 6. Characterization of dendrimer/CEH complexes. (A) Gel retardation assay on G5/CEH and Gal-G5/CEH complexes freshly prepared at different weight ratios. M: the DNA ladder. The stable complexes remained immobile as highlighted. (B) DLS (room temperature) and TEM images of Gal-G5 and freshly prepared Gal-G5/CEH complexes (20:1, w/w). Some Gal-G5 particles are pointed with arrows and Gal-G5/CEH complexes are highlighted in red circles. (C) Hydrodynamic size change of Gal-G5/CEH (20:1, w/w) and G5/CEH (4:1, w/w) at 37 °C in PBS over a period of 24 h. (D) Gel retardation assay on G5/CEH (4:1, w/w) and Gal-G5/CEH (20:1, w/w) following 24 h-incubation 37 °C in PBS or PBS with 10% FBS. Lane 1: the DNA ladder; Lane 2: CEH in PBS; Lane 3: CEH in 10% FBS; Lane 4: G5/CEH in PBS; Lane 5: G5/CEH in 10% FBS; Lane 6: Gal-G5/CEH in PBS; Lane 7: Gal-G5/CEH in 10% FBS. Both G5/CEH and Gal-G5/CEH maintained good colloidal stability and did not release CEH plasmid as highlighted. (For interpretation of the references to colour in this figure legend, the reader is referred to the web version of this article.)

G5 alone to 114.9 nm for Gal-G5/CEH. As shown in the TEM images, the Gal-G5/CEH complexes have a much larger size than Gal-G5.

The colloidal stability of these complexes in salt solution (PBS) as well as in the presence of serum was tested. As shown in Fig. 6C, no significant change in the hydrodynamic diameter of complexes at 37 °C for 24 h suggested that formulation stability of complexes can be maintained for at least 24 h. Fig. 6D showed that naked plasmid DNA (lane 3) was completely digested in the presence of serum likely by nucleases during the 24 h-incubation. In contrast, both types of dendrimer/CEH complexes were not destroyed by serum (lane 5 for G5/CEH and lane 7 for Gal-G5/CEH) and were retained in the loading wells similarly to the corresponding controls in the absence of serum (lane 4 for G5/CEH and lane 6 for Gal-G5/CEH). These results demonstrate that both G5 and Gal-G5 are able to protect the complexed DNA from degradation by serum nucleases and maintain good colloidal stability, supporting their suitable use in *in vitro* and *in vivo* studies.

3.4. Intracellular trafficking of complexes

Effective dissociation and subsequent movement of DNA to the nucleus is critical for expression of the delivered gene. Intracellular localization and dissociation FITC-Gal-G5/Cy3-labeled plasmid and FITC-G5/Cy3 plasmid were examined. After 6 h, Cy3 plasmid was tightly complexed with both vectors. Dissociation of Cy3-plasmid from FITC-Gal-G5 became evident at 24 h, while no appreciable dissociation of Cy3 plasmid and FITC-G5 was observed (Fig. 7, highlighted, clear separation of green FITC-Gal-G5 and red Cy3 plasmid, and some red plasmid also entered the nucleus mediated by FITC-Gal-G5). The dissociation was attributed to the weakened electrostatic interactions between dendrimer and plasmid by long PEG spacer. It was a critical step before released plasmid could further translocate into the nucleus for transcription and translation. Those observations are consistent with facilitated gene transfection delivered by PEGylated-PAMAM dendrimer reported by other researchers [60,61].

3.5. Increased CEH expression and activity in hepatocytes mediated by Gal-G5/CEH complex *in vitro*

To directly examine whether galactose functionalization indeed increases the ability of Gal-G5 to deliver CEH expression vector to

hepatocytes *in vitro*, CEH mRNA expression in hepatocytes was quantified by using RT-qPCR. CEH expression vector where CEH expression was driven by a constitutive Cytomegalo virus (CMV) promoter was used along with empty vector pCMV serving as a control. Fold increase in CEH mRNA expression was determined relative to the expression observed in hepatocytes treated with dendrimer/pCMV. It should be noted that no Ct value was obtained when RNA from hepatocytes treated with G5/pCMV or Gal-G5/pCMV complexes since the PCR probes used were specific for human CEH. As shown in Fig. 8A, expression of CEH delivered by Gal-G5 was about 2- and 6-fold higher than that by G5 ($P < 0.01$) after 24 and 48 h exposure, respectively, demonstrating the higher efficiency of CEH delivery achieved with Gal-G5.

We have earlier demonstrated that increase in hepatic CEH not only leads to the increased hydrolysis of HDL-CE but also increases the flux of cholesterol from HDL-CE to bile acids providing the mechanism underlying the anti-atherosclerotic effects of hepatic CEH [17,44]. The long term objective of developing a non-viral platform for targeted delivery of CEH to the liver is to establish it as a novel anti-atherosclerotic strategy. Towards this goal, it is critical to establish that Gal-G5-delivered CEH is biologically active or functional. To examine whether increased CEH mRNA expression leads to increase in intracellular CE hydrolysis, conversion of HDL-³H-CE to ³H-FC and final conversion of ³H-FC to ³H-BA was monitored. Consistent with the increased CEH mRNA expression, compared to hepatocytes exposed to G5/CEH, significantly higher hydrolysis of HDL-CE was noted in hepatocytes exposed to Gal-G5/CEH complexes (Fig. 8B, $70 \pm 4\%$ versus only $39 \pm 7\%$, $P < 0.05$). Furthermore, increased conversion of HDL-CE derived FC to bile acids was also noted in the hepatocytes treated with Gal-G5/CEH complexes (Fig. 8C, $417 \pm 100\%$ versus $182 \pm 63\%$, $P < 0.05$). Consistent with our earlier data showing increased conversion of HDL-CE to BA following adenovirus-mediated overexpression of CEH or transgenic CEH overexpression in hepatocytes [15,17,44], these data confirm that Gal-G5-mediated delivery of CEH gene leads to the elimination of HDL-CE to BA.

3.6. Enhanced liver-specific delivery *in vivo*

The final step in establishing the validity of galactose functionalized G5 as a platform for delivery of CEH or any other expression vector to the liver to modulate *in vivo* expression, it is important to

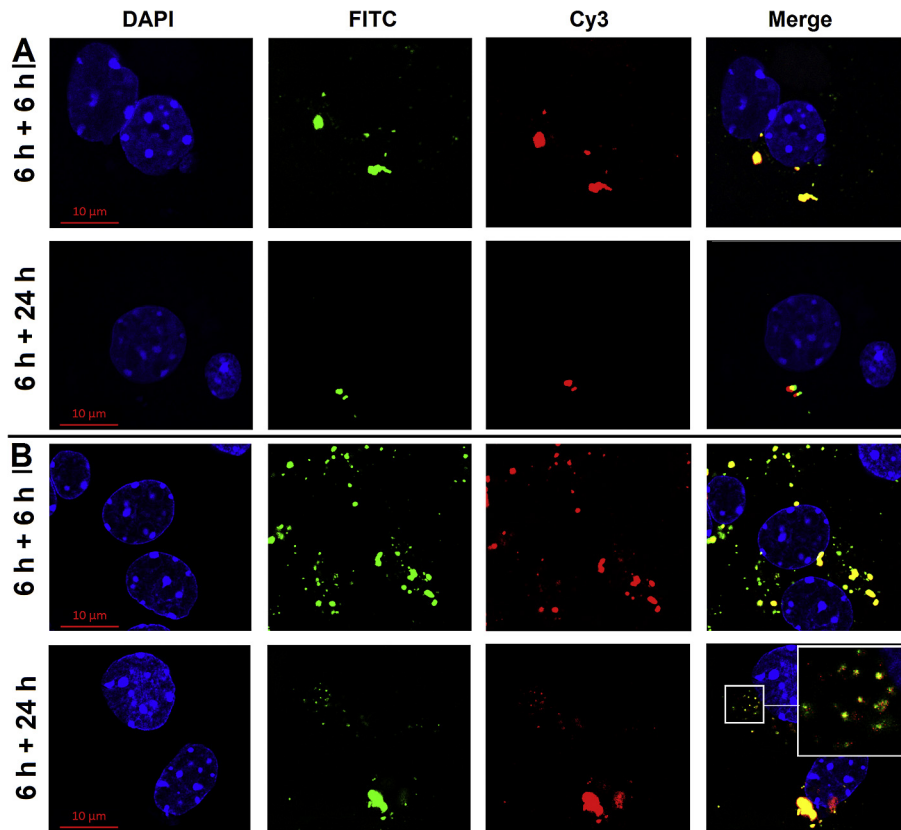


Fig. 7. Intracellular dissociation of Cy3 plasmid from G5 or Gal-G5 in mouse hepatocytes. Primary mouse hepatocytes were incubated with FITC-G5/Cy3 plasmid (4:1, w/w) (A) or FITC-Gal-G5/Cy3 plasmid (20:1, w/w) (B) in William's E medium supplemented with 10% FBS for 6 h. The medium was replaced with fresh medium containing 10% FBS, and the hepatocytes were incubated for an additional 6 or 24 h. At the end of the incubation, the cells were rinsed with DPBS, and the nuclei stained with DAPI and imaged by using confocal microscopy (630 \times). Blue, DAPI; Green, FITC; Red, Cy3. A magnified view of the area outlined by the smaller squared box is presented in the top right corner to show dissociation of plasmid from the carrier. (For interpretation of the references to colour in this figure legend, the reader is referred to the web version of this article.)

not only demonstrate selective uptake by liver but also show that such a delivery does not induce toxicity. For this purpose, time-dependent *in vivo* bio-distribution of IRDye 800CW-labeled Gal-G5/CEH and IRDye 800CW-labeled G5/CEH was monitored after intravenous injection. Fig. 9A shows that IRDye 800CW-labeled Gal-G5/CEH rapidly targeted liver after 1 h intravenous administration and the accumulation gradually increased with highest intensity in liver seen after 48 h. The IRDye 800CW fluorescence intensity persisted for at least 7 days post-administration. This higher liver accumulation of IRDye 800CW-labeled Gal-G5/CEH in comparison to the IRDye 800CW-labeled G5/CEH was consistent with higher *in vitro* hepatocyte uptake described before validating the liver-specific delivery due to galactose functionalization. Compared to G5, PEG modification of galactose resulted in a decrease of the passive reticuloendothelial system (RES) uptake by spleen and renal clearance consistent with known effects of PEGylation, namely, enhanced biocompatibility and non-immunogenicity, and increased blood circulation time by reducing opsonization by proteins and hindering the uptake by macrophages in the RES. Similar accumulation in the RES organs (liver and spleen) was observed in the mice administrated with IRDye 800CW-labeled G5/CEH. Furthermore, obvious accumulation of fluorescent intensity was also observed in kidney from both groups. This is likely due to filtration and secretion of nanosized dendrimer (less than 10 nm) after dissociation of complexes. However, compared with the group treated with IRDye 800CW-labeled G5/CEH, the lower fluorescent signal in kidney from the IRDye 800CW-labeled Gal-G5/CEH-treated group within 48 h was probably attributed to extended circulation time induced by

PEGylation. These data not only are consistent with *in vitro* observation but also clearly demonstrate the ability of Gal-G5 to selectively deliver gene to the liver. The fluorescence intensity of each tissue was quantitatively analyzed using CLx infrared imaging system software and plotted in Fig. 9B.

3.7. Gal-G5 mediated liver-specific delivery increases CEH expression *in vivo*

In vivo CEH gene expression analysis (Fig. 10A) revealed that Gal-G5/CEH resulted in much higher CEH expression (shown as copy number of CEH mRNA) in liver in comparison to the G5/CEH at all three time points. The highest CEH expression in liver was seen in the group-treated with Gal-G5/CEH at 48 h, which was around 3 fold ($P < 0.01$) higher than G5/CEH group. Higher CEH expression in spleen was observed among the mice-treated with G5/CEH post-48 h injection; the decrease in CEH copy number in liver at 72 h could be related to mRNA stability/degradation. CEH expression in other tissues such as heart, lung and kidney was very low for both complexes consistent with low accumulation in both heart and lung. Despite the accumulation of near-infrared (NIR) dye in the kidney likely due to filtration/accumulation of un-complexed or free dendrimer, there was no significant expression of CEH indicating negligible delivery of CEH expression vector. While the Gal-G5/CEH complexes mediated increase in CEH expression seen here is 100-fold lower than the transient adenovirus-mediated CEH expression in liver previously achieved by our lab ($\sim 5 \times 10^6$ copies/ μg total RNA) [17], only a two-fold increase in CEH activity in liver-specific CEH transgenic mice was sufficient to attenuate diet-

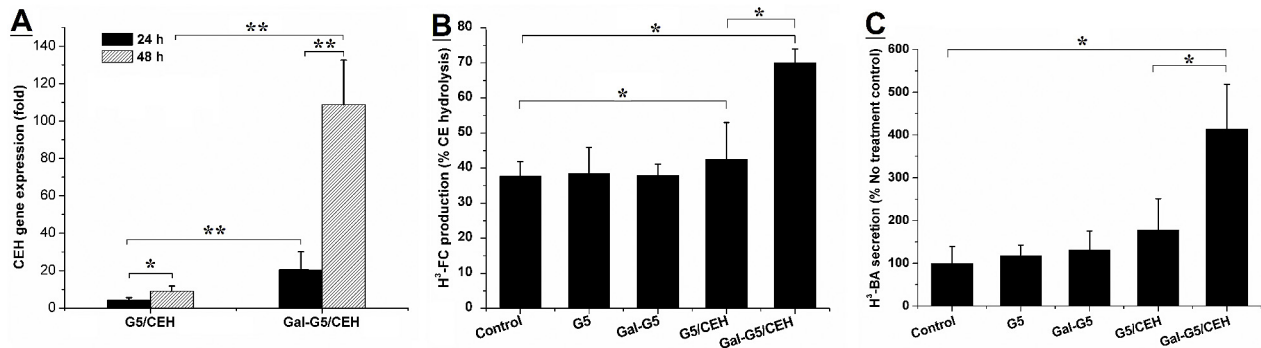


Fig. 8. Delivery of CEH plasmid via Gal-G5 results in increased CEH expression and associated biological activity. (A) CEH expression enhanced by Gal-G/CEH. Primary mouse hepatocytes were treated with G5/pCMV (4:1, w/w) (control), G5/CEH (4:1, w/w), Gal-G5/pCMV (20:1, w/w) (control) or Gal-G5/CEH (20:1, w/w) for 24 h. Following replacement with fresh growth medium, the hepatocytes were incubated for an additional 24 or 48 h. At the end of the treatment, total RNA was isolated and CEH gene expression was determined by using RT-qPCR. CEH expression induced by G5/CEH or Gal-G5/CEH relative to that induced by the corresponding control is presented. $n = 3$, * $P < 0.05$ and ** $P < 0.01$. (B) Intracellular hydrolysis of HDL-CE promoted by Gal-G5/CEH. Primary mouse hepatocytes were incubated with G5, Gal-G5, G5/CEH (4:1, w/w), or Gal-G5/CEH (20:1, w/w) for 24 h. Then the hydrolysis of HDL-³H-CE in each group was monitored. $n = 3$, * $P < 0.05$. (C) The flux of FC to bile acids as a result of CEH-mediated hydrolysis of HDL-³H-CE was assessed by monitoring the appearance of ³H-BA in the culture medium. $n = 3$, * $P < 0.05$.

induced atherosclerosis in *Ldlr*^{-/-} mice [44]. Therefore, this non-viral gene delivery platform still holds promise as a novel alternative with safe application, low cost and simple construction. Liver consists of hepatocytes as well as resident macrophages, i.e., Kupffer cells. Although *in vitro* data showed negligible uptake of Gal-G5 by isolated macrophages, relative expression of CEH was further examined in hepatocytes and Kupffer cells for comparison. As shown in Fig. 10B, there was significantly higher increase in CEH expression in hepatocytes versus Kupffer cells in the mice-treated with Gal-G5/CEH compared to G5/CEH (350-fold higher for Gal-G5/CEH versus 5-fold higher for G5/CEH, $P < 0.01$). Taken together with the *in vitro* data, these results confirm the hepatocyte-specific delivery of CEH by Gal-G5.

3.8. *In vivo* tissue safety of Gal-G5/CEH

Acute systemic toxicity and inflammatory reaction was investigated 24 h after intravenous administration to examine the

biocompatibility of two kinds of complexes. There were no obvious histological differences between the major organs of treated and untreated mice (Fig. 11). Plasma levels of ALT and AST for liver toxicity, BUN for kidney toxicity and TNF- α and IL-6 for induction of inflammatory reaction were determined and the data are summarized in Table 1. Gal-G5/CEH group showed excellent tissue compatibility. No significant differences in these parameters were seen between the Gal-G5/CEH group and the untreated control group. However, significant increases in the levels of ALT, AST and IL-6 were observed in the G5/CEH. These results suggest the toxicity of G5/CEH to tissues or organs including the metabolically active liver. Given the toxicity and low hepatocyte specificity of G5/CEH, only Gal-G5/CEH was evaluated for *in vivo* anti-atherogenic effects.

3.9. Gal-G5 mediated delivery of CEH to liver increases the flux of HDL-CE to bile and feces *in vivo*

The mechanism underlying the anti-atherogenic effects of

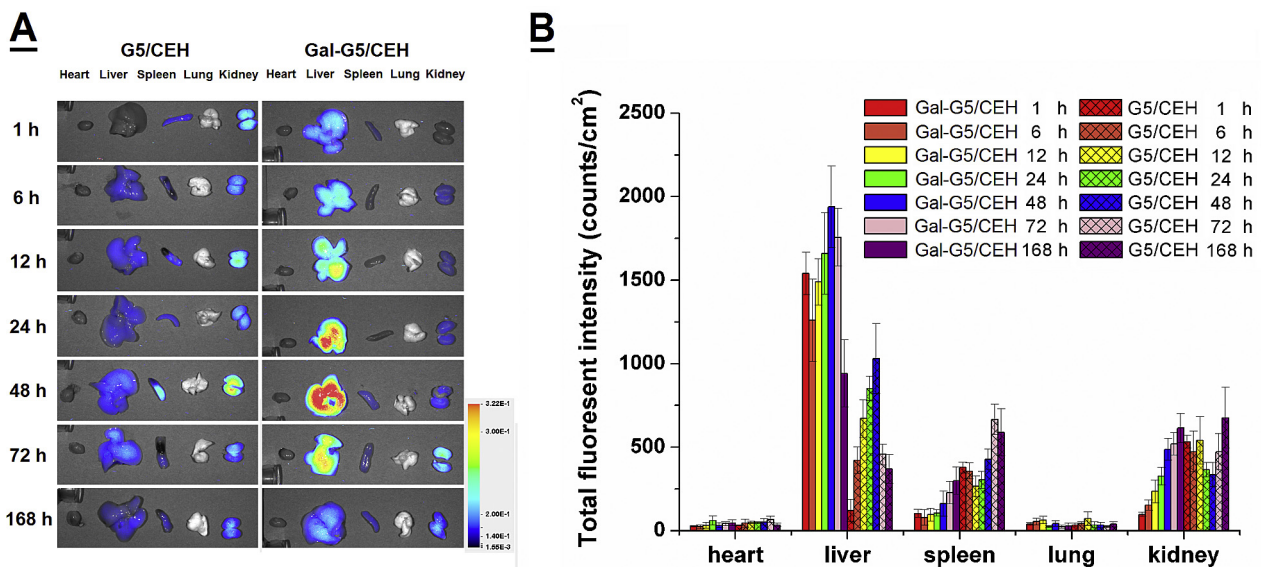


Fig. 9. Enhanced *in vivo* liver uptake of Gal-G5. C57BL/6 mice were administered with IRDye 800CW-labeled Gal-G5/CEH or IRDye 800CW-labeled G5/CEH via tail vein injection. (A) Major organs were harvested at indicated time points and imaged using the Odyssey[®] Fc Imaging System at ex/em = 780/800 nm (heart, liver, spleen, lung and kidney, from left to right). (B) Quantitative analysis of fluorescent signal intensities of the major organs at different time points ($n = 3$).

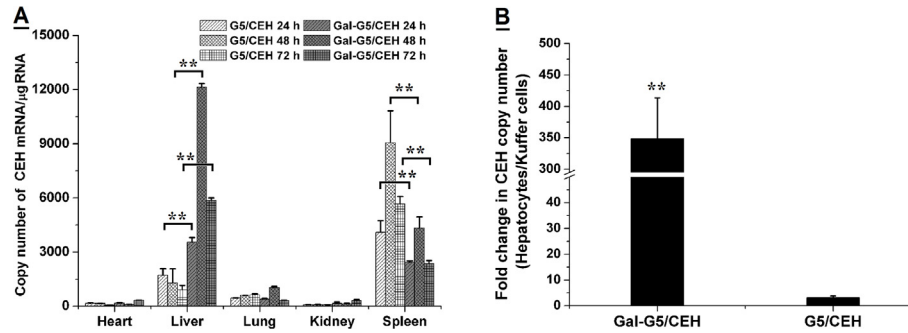


Fig. 10. Enhanced *in vivo* CEH expression in hepatocytes in the liver by Gal-G5/CEH. (A) CEH expression in the major organs at selected time points, i.e., 24, 48 and 72 h post-injection was quantified with RT-qPCR. $n = 3$, ** $P < 0.01$. (B) In a parallel experiment, hepatocytes and Kupffer cells were isolated from the livers of the treated mice at 48 h-post injection, and CEH expression in the isolated cells was quantified with RT-qPCR. A significant increase in CEH expression in hepatocyte relative to that in Kupffer cells was achieved by Gal-G5/CEH. $n = 3$, ** $P < 0.01$.

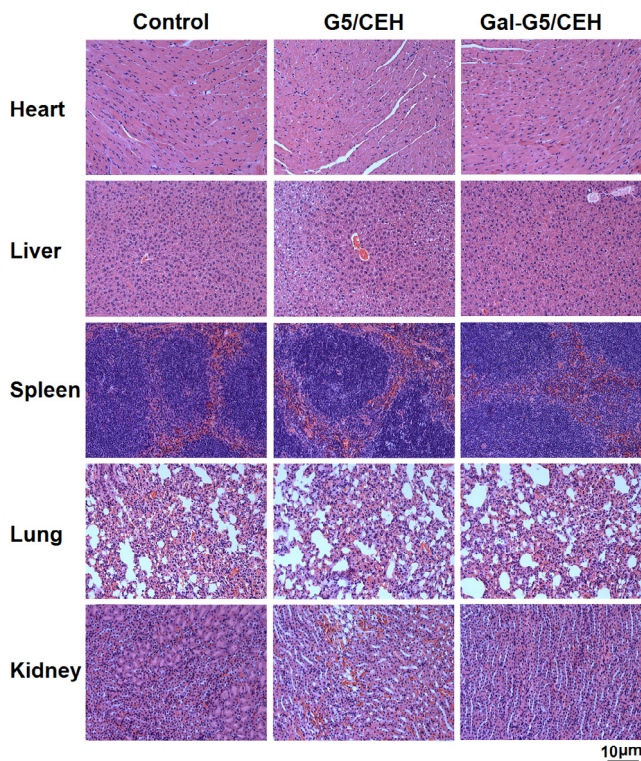


Fig. 11. *In vivo* delivery of CEH by Gal-G5 does not cause tissue toxicity. C57BL/6 mice were injected (i.v.) with Gal-G5 or G5, and major organs were harvested 24 h post-injection. Untreated C57BL/6 mice were used as control. H&E-stained sections of the major organs are shown.

hepatic CEH is its ability to hydrolyze CE delivered by HDL and enhance the flux of resulting FC to bile acids for biliary secretion and elimination in feces. To determine whether Gal-G5-mediated delivery of CEH expression vector modulates this critical step *in vivo*, the flux of radiolabeled-CE from HDL in circulation to the

liver and then to bile acids and feces was monitored. It must be emphasized that the ^3H -label in these studies is associated with the cholesterol moiety of CE permitting the tracking of this label to monitor the hydrolysis of HDL-CE in the liver, its conversion to bile acids and final secretion into feces. As shown in Fig. 12, Gal-G5/CEH significantly increased the CEH expression in liver compared with the blank vector Gal-G5 ($P < 0.01$, Panel A). Following intravenous administration of HDL- ^3H -CE, lower radioactivity in plasma ($P < 0.05$, Panel B) and higher radioactivity in whole liver ($P < 0.05$, Panel C) were observed in the Gal-G5/CEH group, suggesting that the increased CEH expression in the liver increased the clearance of HDL- ^3H -CE from the blood and corresponding increase in uptake by the liver. It should be noted that radioactivity associated with the liver is the sum of ^3H -CE delivered to the liver via HDL receptor SR-BI and the downstream metabolic products of ^3H -CE including ^3H -FC and ^3H -BA. To directly evaluate the effects of increased CEH expression in the liver, radioactivity associated with hepatic FC and BA was determined. Consistent with the increased expression of CEH in mice treated with Gal-G5/CEH complexes, higher radioactivity was associated with hepatic FC and BA ($P < 0.05$, Panel D) indicating that increased CEH expression led to increase in intracellular CE hydrolysis into FC and final conversion of FC to BA. Following synthesis, BA is secreted into bile that is stored in the gall bladder and timely released into the intestine to facilitate digestion. To examine the effects of increased CEH expression in the liver in mediating the flux of cholesterol from HDL to biliary BA, radioactivity associated with BA extracted from gall bladder bile was monitored. Significantly higher level of radiolabel was associated with biliary BA in Gal-G5/CEH complex-treated mice ($P < 0.05$, Panel E and Panel F); there was no significant difference between radiolabel associated with FC. Biliary BA and FC are finally secreted into feces and this represents the only physiological mechanism for final elimination of cholesterol from the body. It is noteworthy that lack of enzymes to cleave the steroid nucleus necessitates the conversion of hydrophobic cholesterol into hydrophilic bile acids by hydroxylation to facilitate elimination in feces. Therefore, any mechanism that can stimulate removal of cholesterol returning to

Table 1
Quantification of hematological biomarkers of hepatic and renal toxicity as well as cytokine biomarkers of immunotoxicity.

Treatment	AST (U/L)	ALT (U/L)	BUN (mg/dL)	IL 6 (ng/mL)	TNF- α (ng/mL)
Control	65 \pm 10.3	34 \pm 3.5	22 \pm 0.6	1.1 \pm 0.10	0.6 \pm 0.11
G5/CEH	315 \pm 114.9**	169 \pm 81.8**	27 \pm 6.1	3.6 \pm 0.20**	0.7 \pm 0.12
Gal-G5/CEH	71 \pm 13.2	37 \pm 8.2	26 \pm 5.6	1.6 \pm 0.05	0.5 \pm 0.05

Note: $n = 3$, ** $P < 0.01$ vs. the control.

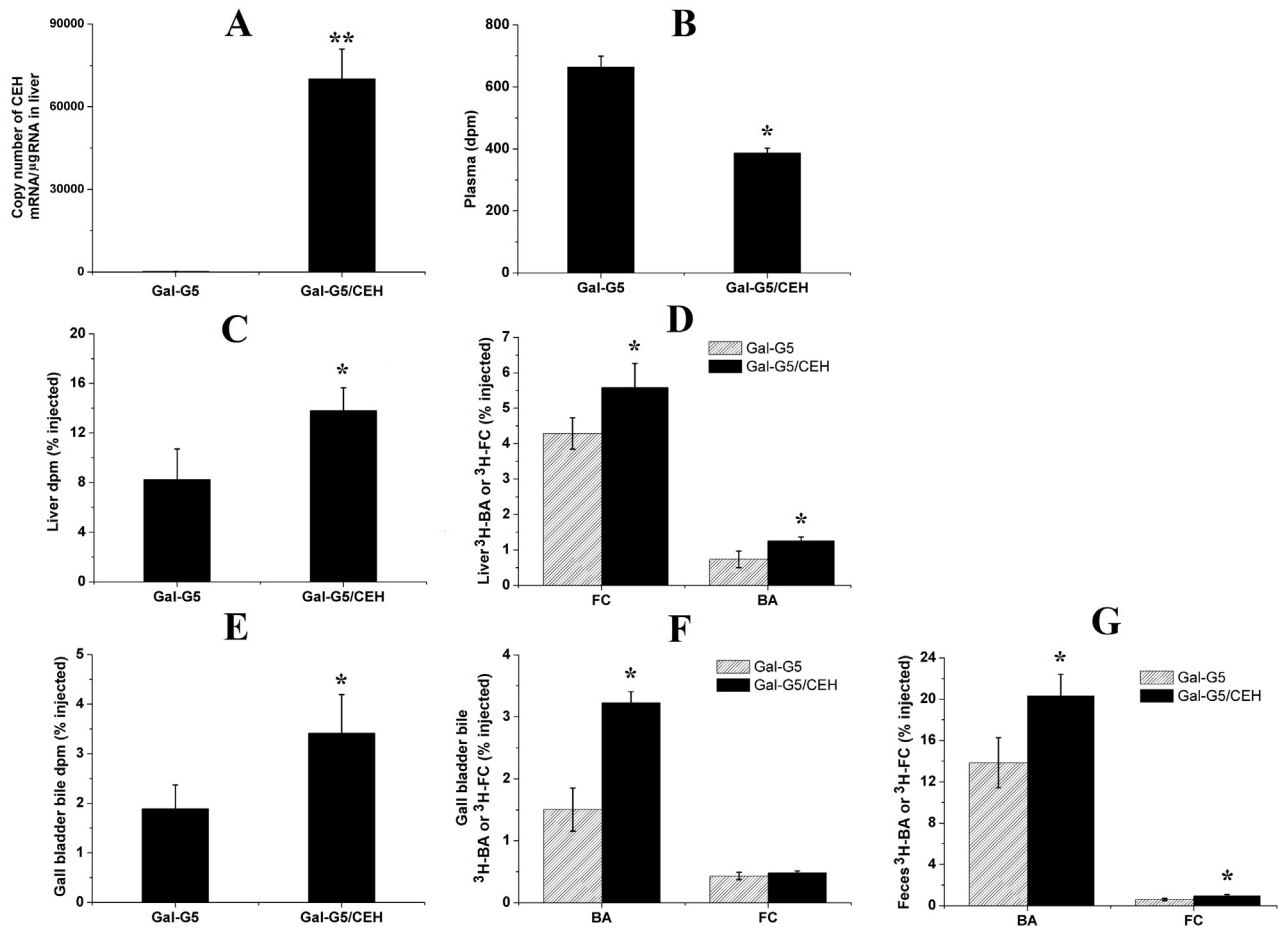


Fig. 12. Increased CEH expression in the liver promotes RCT *in vivo*. WT C57BL/6 mice were administered with Gal-G5 or Gal-G5/CEH via tail vein injection. After 48 h, mice were intravenously injected with [³H]-CE-labeled HDL. After an additional 48 h, blood, liver, gall bladder bile and feces were collected and analyzed. Radioactivity data (n = 3) are presented as the percentage of the total injected radiolabeled dose. (A) CEH expression in the liver (**P < 0.01); (B) radioactivity in plasma (*P < 0.05); (C) total radioactivity in the liver (*P < 0.05); (D) ³H-FC and ³H-BA in the liver (*P < 0.05); (E) total radioactivity in gall bladder bile (*P < 0.05); (F) ³H-FC and ³H-BA in gall bladder bile (*P < 0.05); (G) ³H-FC and ³H-BA in feces (*P < 0.05).

the liver from the peripheral tissues (as CE in HDL particle), including arterial-plaque associated macrophage foam cells, will potentially reduce cholesterol burden and be anti-atherogenic. Therefore, as a final step, effects of Gal-G5 delivered CEH expression vector on fecal elimination of cholesterol derived from HDL was monitored. Significantly higher radioactivity was also associated with fecal BA and FC in mice injected with Gal-G5/CEH complex compared with mice injected with Gal-G5 (P < 0.05, Panel G). These data are consistent with earlier studies from our laboratory showing increased flux of HDL-CE to bile and feces by hepatic over-expression of CEH [15,17,44,48] that promotes intracellular hydrolysis of HDL delivered CE and thus enhances the elimination of cholesterol from the body. Indeed, transgenic over expression of CEH attenuates atherosclerosis in *Ldlr*^{-/-} mice and these data provide a non-genetic/non-viral approach to enhancing the expression of CEH in the liver as a potentially novel anti-atherogenic strategy.

4. Conclusions

Inhibition of pathological processes central to the development of disease, by pharmacologically active small molecules [62] or genetic manipulation by small interfering RNA (siRNA)/microRNA (miRNA)/antisense oligonucleotides (ASOs) [63–65], is the most widely accepted strategy to reduce the progression of diseases.

However, enhancing an endogenous biological process that is necessary for the prevention of disease progression, and more importantly the reversal of the disease, has proven to be challenging mainly because of the lack of suitable platforms for the introduction of the critical gene required to increase the affected pathway. Based on the significant residual CVD risk present despite reaching the target LDL cholesterol levels and failure of risk reduction by merely increasing HDL cholesterol levels has shifted the paradigm from lipoprotein associated cholesterol to flux of cholesterol from arterial plaque associated macrophages to liver and final elimination from the body [66]. The fact that cholesterol is carried within the lipoproteins as CE but only FC is secreted in bile either directly or following conversion to bile acids underscores the importance of hepatic CE hydrolysis and earlier studies from our laboratory have established the anti-atherogenic role of hepatic CEH. Currently, endogenous regulation of CEH remains largely unknown in mice or humans although reduced CEH expression is reported in human carotid artery plaques [4]. With the objective to address the as yet unmet need for novel strategies for enhancing the removal of cholesterol from body, the data presented herein demonstrates the suitability of Gal-G5 to deliver CEH to the liver and increase the flux of cholesterol from HDL-CE to FC and bile acids by increasing CE hydrolysis within the hepatocytes. Furthermore, functionalization of G5 with galactose not only increases liver-specific delivery, but use of long PEG spacer for galactose also

reduces the toxicity associated with high positive charges on the surface of unmodified G5. The development of this relatively non-toxic and efficient liver-specific gene delivery platform is an encouraging step towards the clinical translation of strategies based on enhancing removal of cholesterol from the body to reduce the existing atherosclerotic plaque burden (or plaque regression) for which no therapeutics are currently available. It is noteworthy that hepatocyte-specific CEH over-expression significantly attenuates western diet-induced atherosclerosis without having any effect on plasma lipoprotein profile [44]. Future studies will be focused on the pre-clinical evaluation of Gal-G5/CEH-mediated increase in cholesterol elimination from the body and its impact on reducing atherosclerotic plaque burden.

Acknowledgements

This work was supported, in part, by VCU's CTSA (UL1TR000058 from the National Center for Advancing Translational Sciences) and the CCTR Endowment Fund of Virginia Commonwealth University to HY and SG as well as NSF CAREER award CBET0954957 (HY).

References

- [1] R.B. D'Agostino, M.W. Russell, D.M. Huse, R.C. Ellison, H. Silbershatz, P.W. Wilson, S.C. Hartz, Primary and subsequent coronary risk appraisal: new results from the Framingham study, *Am. Heart J.* 139 (2) (2000) 272–281.
- [2] P. Libby, Inflammation in atherosclerosis, *Arterioscler. Thromb. Vasc. Biol.* 32 (9) (2012) 2045–2051.
- [3] K.J. Moore, F.J. Sheedy, E.A. Fisher, Macrophages in atherosclerosis: a dynamic balance, *Nat. Rev. Immunol.* 13 (10) (2013) 709–721.
- [4] S. Ghosh, Macrophage cholesterol homeostasis and metabolic diseases: critical role of cholesteryl ester mobilization, *Expert Rev. Cardiovasc. Ther.* 9 (3) (2011) 329–340.
- [5] S. Ghosh, B. Zhao, J. Bie, J. Song, Macrophage cholesteryl ester mobilization and atherosclerosis, *Vasc. Pharmacol.* 52 (1) (2010) 1–10.
- [6] W.J. Mulder, F.A. Jaffer, Z.A. Fayad, M. Nahrendorf, Imaging and nanomedicine in inflammatory atherosclerosis, *Sci. Transl. Med.* 6 (239) (2014) 239sr1.
- [7] S. Ghosh, B. Zhao, J. Bie, J. Song, Role of cholesteryl ester hydrolase in atherosclerosis, *Clin. Lipidol.* 4 (5) (2009) 573–585.
- [8] S. Ghosh, J. Bie, J. Wang, Q. Yuan, S.S. Ghosh, Cholesterol removal from plaques and elimination from the body: change in paradigm to reduce risk for heart disease, *Clin. Lipidol.* 9 (4) (2014) 429–440.
- [9] A. Rohatgi, A. Khera, J.D. Berry, E.G. Givens, C.R. Ayers, K.E. Wedin, I.J. Neeland, I.S. Yuhanna, D.R. Rader, J.A. de Lemos, HDL cholesterol efflux capacity and incident cardiovascular events, *N. Engl. J. Med.* 371 (25) (2014) 2383–2393.
- [10] D. Saleheen, R. Scott, S. Javad, W. Zhao, A. Rodrigues, A. Picataggi, D. Lukmanova, M.L. Mucksavage, R. Luben, J. Billheimer, Association of HDL cholesterol efflux capacity with incident coronary heart disease events: a prospective case-control study, *Lancet Diabetes Endocrinol.* 3 (7) (2015) 507–513.
- [11] A.V. Khera, M. Cuchel, M. de la Llera-Moya, A. Rodrigues, M.F. Burke, K. Jafri, B.C. French, J.A. Phillips, M.L. Mucksavage, R.L. Wilensky, Cholesterol efflux capacity, high-density lipoprotein function, and atherosclerosis, *N. Engl. J. Med.* 364 (2) (2011) 127–135.
- [12] S. Ghosh, Cholesteryl ester hydrolase in human monocyte/macrophage: cloning, sequencing, and expression of full-length cDNA, *Physiol. Genomics* 2 (1) (2000) 1–8.
- [13] B. Zhao, B.J. Fisher, R.W.S. Clair, L.L. Rudel, S. Ghosh, Redistribution of macrophage cholesteryl ester hydrolase from cytoplasm to lipid droplets upon lipid loading, *J. Lipid Res.* 46 (10) (2005) 2114–2121.
- [14] M.A. Connelly, D.L. Williams, Scavenger receptor BI: a scavenger receptor with a mission to transport high density lipoprotein lipids, *Curr. Opin. Lipidol.* 15 (3) (2004) 287–295.
- [15] J. Bie, J. Wang, K.E. Marqueen, R. Osborne, G. Kakiyama, W. Korzun, S.S. Ghosh, S. Ghosh, Liver-specific cholesteryl ester hydrolase deficiency attenuates sterol elimination in the feces and increases atherosclerosis in *ldlr*^{-/-} mice, *Arterioscler. Thromb. Vasc. Biol.* 33 (8) (2013) 1795–1802.
- [16] J. Bie, B. Zhao, S. Ghosh, Atherosclerotic lesion progression is attenuated by reconstitution with bone marrow from macrophage-specific cholesteryl ester hydrolase transgenic mice, *Am. J. Physiol. Regul. Integr. Comp. Physiol.* 301 (4) (2011) R967–R974.
- [17] B. Zhao, J. Song, S. Ghosh, Hepatic overexpression of cholesteryl ester hydrolase enhances cholesterol elimination and in vivo reverse cholesterol transport, *J. Lipid Res.* 49 (10) (2008) 2212–2217.
- [18] G. Charach, I. Grosskopf, A. Rabinovich, M. Shochat, M. Weintraub, P. Rabinovich, The association of bile acid excretion and atherosclerotic coronary artery disease, *Ther. Adv. Gastroenterol.* 4 (2) (2011) 95–101.
- [19] H. Simonen, T.A. Miettinen, Coronary artery disease and bile acid synthesis in familial hypercholesterolemia, *Atherosclerosis* 63 (2–3) (1987) 159–166.
- [20] H. Yang, J.J. Morris, S.T. Lopina, Polyethylene glycol–polyamidoamine dendritic micelle as solubility enhancer and the effect of the length of polyethylene glycol arms on the solubility of pyrene in water, *J. Colloid Interface Sci.* 273 (1) (2004) 148–154.
- [21] E.R. Figueroa, A.Y. Lin, J. Yan, L. Luo, A.E. Foster, R.A. Drezek, Optimization of PAMAM-gold nanoparticle conjugation for gene therapy, *Biomaterials* 35 (5) (2014) 1725–1734.
- [22] S. Mallick, J.S. Choi, Polyamidoamine (PAMAM) dendrimers modified with short oligopeptides for early endosomal escape and enhanced gene delivery, *Int. J. Pharm.* 492 (1) (2015) 233–243.
- [23] Q. Yuan, W.A. Yeudall, H. Yang, PEGylated polyamidoamine dendrimers with bis-aryl hydrazone linkages for enhanced gene delivery, *Biomacromolecules* 11 (8) (2010) 1940–1947.
- [24] H. Liu, H. Wang, Y. Xu, R. Guo, S. Wen, Y. Huang, W. Liu, M. Shen, J. Zhao, G. Zhang, Lactobionic acid-modified dendrimer-entrapped gold nanoparticles for targeted computed tomography imaging of human hepatocellular carcinoma, *ACS Appl. Mater. Interfaces* 6 (9) (2014) 6944–6953.
- [25] Q. Yuan, Y. Fu, W.J. Kao, D. Janigro, H. Yang, Transbuccal delivery of CNS therapeutic nanoparticles: synthesis, characterization, and in vitro permeation studies, *ACS Chem. Neurosci.* 2 (11) (2011) 676–683.
- [26] W. Ke, K. Shao, R. Huang, L. Han, Y. Liu, J. Li, Y. Kuang, L. Ye, J. Lou, C. Jiang, Gene delivery targeted to the brain using an Angiopep-conjugated poly-ethyleneglycol-modified polyamidoamine dendrimer, *Biomaterials* 30 (36) (2009) 6976–6985.
- [27] H. Wang, L. Zheng, C. Peng, M. Shen, X. Shi, G. Zhang, Folic acid-modified dendrimer-entrapped gold nanoparticles as nanoprobes for targeted CT imaging of human lung adenocarcinoma, *Biomaterials* 34 (2) (2013) 470–480.
- [28] Y.-N. Zhang, W. Poon, A.J. Tavares, I.D. McGilvray, W.C. Chan, Nanoparticle-liver interactions: cellular uptake and hepatobiliary elimination, *J. Control. Release* 240 (2016) 332–348.
- [29] L. Li, H. Wang, Z.Y. Ong, K. Xu, P.L.R. Ee, S. Zheng, J.L. Hedrick, Y.-Y. Yang, Polymer- and lipid-based nanoparticle therapeutics for the treatment of liver diseases, *Nano Today* 5 (4) (2010) 296–312.
- [30] J.A. Hubbell, A. Chilkoti, Nanomaterials for drug delivery, *Science* 337 (6092) (2012) 303–305.
- [31] X.-C. Yang, Y.-L. Niu, N.-N. Zhao, C. Mao, F.-J. Xu, A biocleavable pullulan-based vector via ATRP for liver cell-targeting gene delivery, *Biomaterials* 35 (12) (2014) 3873–3884.
- [32] Y. Ren, R.Q. Li, Y.R. Cai, T. Xia, M. Yang, F.J. Xu, Effective codelivery of lncRNA and pDNA by pullulan-based nanovectors for promising therapy of hepatocellular carcinoma, *Adv. Funct. Mater.* 26 (40) (2016) 7314–7325.
- [33] Y. Hu, M.T. Haynes, Y. Wang, F. Liu, L. Huang, A highly efficient synthetic vector: nonhydrodynamic delivery of DNA to hepatocyte nuclei in vivo, *ACS Nano* 7 (6) (2013) 5376–5384.
- [34] Y. Tachibana, M.C. Munisso, W. Kamata, M. Kitagawa, M. Harada-Shiba, T. Yamaoka, Quick nuclear transportation of siRNA and in vivo hepatic ApoB gene silencing with galactose-bearing polymeric carrier, *J. Biotechnol.* 175 (2014) 15–21.
- [35] M.H. Lee, J.H. Han, P.-S. Kwon, S. Bhuniya, J.Y. Kim, J.L. Sessler, C. Kang, J.S. Kim, Hepatocyte-targeting single galactose-appended naphthalimide: a tool for intracellular thiol imaging in vivo, *J. Am. Chem. Soc.* 134 (2) (2012) 1316–1322.
- [36] J. Huang, F. Gao, X. Tang, J. Yu, D. Wang, S. Liu, Y. Li, Liver-targeting doxorubicin-conjugated polymeric prodrug with pH-triggered drug release profile, *Polym. Int.* 59 (10) (2010) 1390–1396.
- [37] F. Fu, Y. Wu, J. Zhu, S. Wen, M. Shen, X. Shi, Multifunctional lactobionic acid-modified dendrimers for targeted drug delivery to liver cancer cells: investigating the role played by PEG spacer, *ACS Appl. Mater. Interfaces* 6 (18) (2014) 16416–16425.
- [38] B. Zhao, R. Natarajan, S. Ghosh, Human liver cholesteryl ester hydrolase: cloning, molecular characterization, and role in cellular cholesterol homeostasis, *Physiol. Genomics* 23 (3) (2005) 304–310.
- [39] J. Wang, J. Bie, S. Ghosh, Intracellular cholesterol transport proteins enhance hydrolysis of HDL-delivered cholesteryl esters and facilitate preferential elimination of resulting cholesterol into bile, *J. Lipid Res.* (2016) jlr.M069682.
- [40] H. Yang, W.J. Kao, Synthesis and characterization of nanoscale dendritic RGD clusters for potential applications in tissue engineering and drug delivery, *Int. J. Nanomed.* 2 (1) (2007) 89–99.
- [41] T.-H. Tran, S. Krishnan, M.M. Amiji, MicroRNA-223 induced repolarization of peritoneal macrophages using CD44 targeting hyaluronic acid nanoparticles for anti-inflammatory effects, *PLoS One* 11 (5) (2016) e0152024.
- [42] L. Xu, S. Kittrell, W.A. Yeudall, H. Yang, Folic acid-decorated polyamidoamine dendrimer mediates selective uptake and high expression of genes in head and neck cancer cells, *Nanomedicine* 11 (22) (2016) 2959–2973.
- [43] B. Zhao, J. Bie, J. Wang, S.A. Marqueen, S. Ghosh, Identification of a novel intracellular cholesteryl ester hydrolase (carboxylesterase 3) in human macrophages: compensatory increase in its expression after carboxylesterase 1 silencing, *Am. J. Physiol. Cell Physiol.* 303 (4) (2012) C427–C435.
- [44] J. Bie, J. Wang, Q. Yuan, G. Kakiyama, S.S. Ghosh, S. Ghosh, Liver-specific transgenic expression of cholesteryl ester hydrolase reduces atherosclerosis in *ldlr*^{-/-} mice, *J. Lipid Res.* 55 (4) (2014) 729–738.
- [45] K. Kim, J.H. Kim, H. Park, Y.-S. Kim, K. Park, H. Nam, S. Lee, J.H. Park, R.-W. Park, I.-S. Kim, Tumor-homing multifunctional nanoparticles for cancer theragnosis: simultaneous diagnosis, drug delivery, and therapeutic monitoring,

- J. Control. Release 146 (2) (2010) 219–227.
- [46] Y. Bi, L. Liu, Y. Lu, T. Sun, C. Shen, X. Chen, Q. Chen, S. An, X. He, C. Ruan, T7 peptide-functionalized PEG-PLGA micelles loading with carmustine for targeting therapy of glioma, *ACS Appl. Mater. Interfaces* 8 (41) (2016) 27465–27473.
- [47] L.J. Cruz, M.A. Stammes, I. Que, E.R. van Beek, V.T. Knol-Blankevoort, T.J. Snoeks, A. Chan, E.L. Kaijzel, C.W. Löwik, Effect of PLGA NP size on efficiency to target traumatic brain injury, *J. Control. Release* 223 (2016) 31–41.
- [48] B. Zhao, J. Song, W.N. Chow, R.W.S. Clair, L.L. Rudel, S. Ghosh, Macrophage-specific transgenic expression of cholesteryl ester hydrolase significantly reduces atherosclerosis and lesion necrosis in Ldlr^{-/-} mice, *J. Clin. Invest.* 117 (10) (2007) 2983–2992.
- [49] E.G. Bligh, W.J. Dyer, A rapid method of total lipid extraction and purification, *Can. J. Biochem. Physiol.* 37 (8) (1959) 911–917.
- [50] R. Jevprasesphant, J. Penny, R. Jalal, D. Attwood, N. McKeown, A. D'emanuele, The influence of surface modification on the cytotoxicity of PAMAM dendrimers, *Int. J. Pharm.* 252 (1) (2003) 263–266.
- [51] W. Wang, W. Xiong, J. Wan, X. Sun, H. Xu, X. Yang, The decrease of PAMAM dendrimer-induced cytotoxicity by PEGylation via attenuation of oxidative stress, *Nanotechnology* 20 (10) (2009) 105103.
- [52] H. Yang, S.T. Lopina, L.P. DiPersio, S.P. Schmidt, Stealth dendrimers for drug delivery: correlation between PEGylation, cytocompatibility, and drug payload, *J. Mater. Sci. Mater. Med.* 19 (5) (2008) 1991–1997.
- [53] S.K. Kim, K.M. Park, K. Singha, J. Kim, Y. Ahn, K. Kim, W.J. Kim, Galactosylated cucurbituril-inclusion polyplex for hepatocyte-targeted gene delivery, *Chem. Commun.* 46 (5) (2010) 692–694.
- [54] A. Lakshminarayanan, B.U. Reddy, N. Raghav, V.K. Ravi, A. Kumar, P.K. Maiti, A. Sood, N. Jayaraman, S. Das, A galactose-functionalized dendritic siRNA-nanovector to potentiate hepatitis C inhibition in liver cells, *Nanoscale* 7 (40) (2015) 16921–16931.
- [55] C.H. Lai, C.Y. Lin, H.T. Wu, H.S. Chan, Y.J. Chuang, C.T. Chen, C.C. Lin, Galactose encapsulated multifunctional nanoparticle for HepG2 cell internalization, *Adv. Funct. Mater.* 20 (22) (2010) 3948–3958.
- [56] A.S. Zahr, C.A. Davis, M.V. Pishko, Macrophage uptake of core-shell nanoparticles surface modified with poly (ethylene glycol), *Langmuir* 22 (19) (2006) 8178–8185.
- [57] Y. Zhang, N. Kohler, M. Zhang, Surface modification of superparamagnetic magnetite nanoparticles and their intracellular uptake, *Biomaterials* 23 (7) (2002) 1553–1561.
- [58] J. Lipka, M. Semmler-Behnke, R.A. Sperling, A. Wenk, S. Takenaka, C. Schleh, T. Kissel, W.J. Parak, W.G. Kreyling, Biodistribution of PEG-modified gold nanoparticles following intratracheal instillation and intravenous injection, *Biomaterials* 31 (25) (2010) 6574–6581.
- [59] B. Pelaz, P. del Pino, P. Maffre, R. Hartmann, M. Gallego, S. Rivera-Fernandez, J.M. de la Fuente, G.U. Nienhaus, W.J. Parak, Surface functionalization of nanoparticles with polyethylene glycol: effects on protein adsorption and cellular uptake, *ACS Nano* 9 (7) (2015) 6996–7008.
- [60] D. Luong, P. Kesharwani, R. Deshmukh, M.C.I.M. Amin, U. Gupta, K. Greish, A.K. Iyer, PEGylated PAMAM dendrimers: enhancing efficacy and mitigating toxicity for effective anticancer drug and gene delivery, *Acta Biomater.* 43 (2016) 14–29.
- [61] W. Shen, M.A. van Dongen, Y. Han, M. Yu, Y. Li, G. Liu, M.M.B. Holl, R. Qi, The role of caveolin-1 and syndecan-4 in the internalization of PEGylated PAMAM dendrimer polyplexes into myoblast and hepatic cells, *Eur. J. Pharm. Biopharm.* 88 (3) (2014) 658–663.
- [62] L. Liu, H. He, M. Zhang, S. Zhang, W. Zhang, J. Liu, Hyaluronic acid-decorated reconstituted high density lipoprotein targeting atherosclerotic lesions, *Biomaterials* 35 (27) (2014) 8002–8014.
- [63] T. Sun, R. Simmons, D. Huo, B. Pang, X. Zhao, C.W. Kim, H. Jo, Y. Xia, Targeted delivery of anti-mir-712 by VCAM1-binding Au nanospheres for atherosclerosis therapy, *ChemNanoMat* 2 (5) (2016) 400–406.
- [64] J.A. Wolfram, J.K. Donahue, Gene therapy to treat cardiovascular disease, *J. Am. Heart Assoc.* 2 (4) (2013) e000119.
- [65] G. Fredman, N. Kamaly, S. Spolitu, J. Milton, D. Ghorpade, R. Chiasson, G. Kuriakose, M. Perretti, O. Farokhzad, I. Tabas, Targeted nanoparticles containing the proresolving peptide Ac2-26 protect against advanced atherosclerosis in hypercholesterolemic mice, *Sci. Transl. Med.* 7 (275) (2015), 275ra20.
- [66] S. Tuteja, D.J. Rader, High-density lipoproteins in the prevention of cardiovascular disease: changing the paradigm, *Clin. Pharmacol. Ther.* 96 (1) (2014) 48–56.